JOURNAL OF PROPULSION AND POWER
Vol. 20, No. 6, November–December 2004

Mach Number/Surface Roughness Effects on Symmetric Transonic Turbine Airfoil Aerodynamic Losses

Qiang Zhang* and Phillip M. Ligrani†
University of Utah, Salt Lake City, Utah 84112-9208

The effects of surface roughness and Mach number on the aerodynamic performance of turbine airfoils are investigated in compressible, high-speed flows with exit freestream Mach numbers of 0.6, 0.8, and 0.9 and three different inlet turbulence intensity levels of 0.9, 5.5, and 16.2%. Three symmetric airfoils, each with the same shape and exterior dimensions, are employed with different rough surfaces. The nonuniform, irregular, three-dimensional roughness is characterized using the equivalent sand grain roughness size. Increased surface roughness size and increasing freestream Mach number produce larger magnitudes of nondimensional total pressure loss coefficients. Magnitudes of integrated aerodynamic losses change by a much larger amount as either the freestream Mach number or turbulence intensity are altered, when the airfoil is roughened (compared to smooth airfoil results). This is partially a result of the thicker boundary layers, which develop over the roughened surfaces giving greater blockage and less expansion of the flow through the airfoil passage. As a result, total pressure losses indicate that oblique shock waves are present at the trailing edge of the airfoil (with transonic passage flow) when the airfoil is smooth, which are not present when the airfoil surfaces become roughened.

Nomenclature

C_p	=	total pressure loss coefficient, $(P_{0i} - P_{0e})/P_{0i}$
$C_{p,\infty}$	=	total pressure loss coefficient in the freestream, $(P_{0i} - P_{0e,\infty})/P_{0i}$
c	=	chord length of airfoil
KE	=	normalized kinetic energy, $(P_{0e} - P_{se})/(P_{0e} - P_{se})_\infty$
k	=	mean roughness height
k_s	=	equivalent sand grain roughness
k_s^+	=	normalized sand grain roughness just before the airfoil trailing edge, $k_s V_\tau/\nu$
M	=	local Mach number along the airfoil
M_e	=	exit local Mach number at one chord length downstream of the airfoil
$M_{e,\infty}$	=	exit freestream Mach number at one chord length downstream of the airfoil
P_{se}	=	exit static pressure
P_0	=	stagnation pressure
P_{0e}	=	exit local stagnation pressure
$P_{0e,\infty}$	=	exit freestream stagnation pressure
P_{0i}	=	inlet stagnation pressure
p	=	airfoil passage effective pitch
S	=	rough surface flat reference area
S_f	=	total roughness frontal area
S_s	=	total roughness windward wetted surface area
Tu	=	longitudinal turbulence intensity at test section inlet
V_τ	=	friction velocity
x	=	linear distance along airfoil centerline from airfoil leading edge
y	=	normal coordinate measured from airfoil centerline
Λ_s	=	roughness parameter
ν	=	kinetic viscosity

Received 28 October 2003; revision received 21 April 2004; accepted for publication 13 April 2004.

*Graduate Student, Convective Heat Transfer Laboratory, Department of Mechanical Engineering.

†Professor, Convective Heat Transfer Laboratory, Department of Mechanical Engineering.

Introduction

THE influence of surface roughness on adjacent flow behavior has been of interest for researchers for almost 100 years. The use of equivalent sand grain roughness size k_s to characterize and quantify rough surfaces was first proposed and utilized by Nikuradse[1] and Schlichting.[2] This quantity represents the size of sand grains, which give the same skin-friction coefficients in internal passages as the roughness being evaluated. This measure of roughness size continues to be used widely in empirical correlation equations (which are based on experimental data) to represent rough surface behavior and for closure models employed in a variety of numerical prediction codes. Sigal and Danberg[3,4] made important advances in accounting for roughness geometry considerations for uniformly shaped roughness elements spread in a uniform pattern over a test surface. For this type of two-dimensional roughness, the authors provide equations for the dependence of the ratio of equivalent sand grain roughness to mean roughness height k_s/k on a roughness parameter Λ_s, which is determined from roughness geometry. Van Rij et al.[5] give a modified version of the Sigal and Danberg correlation for the dependence of k_s/k on Λ_s for randomly placed, nonuniform, three-dimensional roughness with irregular geometry and arrangement. Also described are analytic procedures for determination of roughness height k and Λ_s from roughness geometry. With this approach, magnitudes of equivalent sand grain roughness size k_s are determined entirely from three-dimensional roughness geometry. Van Rij et al.[5] verify the results, and analytic procedures employed, using 1) experimental results obtained with the same type of three-dimensional roughness and 2) analytic descriptions of the geometry of uniformly shaped roughness elements arranged in a regular pattern on the test surface.

In a paper published in 1975, Bammert and Sandstede[6] describe the influences of different manufacturing tolerances and turbine airfoil surface roughness characteristics on the overall performance of turbines and indicate that losses increase sharply above a certain roughness size. Measurements of the boundary-layer development along blades with varying roughness are carried out by the same authors,[7] who show that rough surface momentum thickness is up to three times greater than values present in boundary layers on smooth surfaces. Kind et al.[8] investigate the effects of partial roughness coverage of the blade surfaces and conclude that roughness on the suction surface can cause large increases in profile losses. Flat plate surfaces with cone-shaped elements are used by Bogard et al.[9] to simulate the roughness present on vane surfaces; they indicate that the effects of surface roughness and high free-stream turbulence are

additive with regard to heat transfer. Abuaf et al.[10] find that tumbling and polishing reduce the average roughness size and improve overall performance when they quantify heat transfer and aerodynamic performance characteristics of turbine airfoils with different surface finish treatments. From experiments conducted using a compressor cascade, Leipold et al.[11] indicate that surface roughness has no effect on the presence or location of laminar separation, but that roughness causes the turbulent boundary layer to separate at locations farther upstream at higher Reynolds numbers. Guo et al.[12] report on the influences of localized pin-shaped surface roughness on heat transfer and aerodynamic performance of a fully film-cooled engine aerofoil, and indicate that substantial loss increases are present when the pins are located on the pressure side of the airfoil.

Of the investigations that also examine the effects of augmented freestream turbulence levels, Gregory-Smith and Cleak[13] show that the mean flowfield is not affected significantly by inlet turbulence intensity levels as high as 5%. Hoffs et al.[14] investigate different surface roughness characteristics at different Reynolds numbers on a turbine airfoil, with turbulence intensity levels as high as 10%, and show that heat transfer gradually increases and that laminar-to-turbulent transition moves upstream as the Reynolds number and turbulent intensity increase. The effects of strong secondary flows, laminar-to-turbulent transition, and variations near the stagnation line are investigated by Giel et al.[15] using an active blowing grid of square bars as a turbulence generator at the entrance of a transonic cascade. Boyle et al.[16] provide turbine vane aerodynamic data at low Reynolds numbers taken at midspan locations downstream of a linear cascade with inlet turbulence intensity levels as high as 10%. Nix et al.[17] describe the development of a grid that produces freestream turbulence characteristics that are similar to ones produced by the flow exiting combustors of advanced gas turbine engines.

In a study of aerodynamic losses downstream of subsonic turbine airfoil with no film cooling, Ames and Plesniak[18] demonstrate important connections between wake growth and the level of freestream turbulence. Jouini et al.[19] present detailed measurements of midspan aerodynamic performance characteristics of a transonic turbine cascade at off-design conditions. Measurements of blade loading, exit flow angles, and trailing-edge base pressures at different Mach numbers show that profile losses at transonic conditions are closely related to base pressure behavior. Radomsky and Thole[20] present measurements of time-averaged velocity components and Reynolds stresses along a turbine stator vane at elevated freestream turbulence levels and present data that show that transition occurs farther upstream on the suction side, as the freestream turbulence level increases. Total pressure loss measurements, for a high-pressure turbine vane by Christopher et al.,[21] increase approximately with the square change of the exit Mach number. Coton et al.[22] investigate the effects of Reynolds number and Mach number on the profile losses of a conventional low-pressure turbine rotor cascade and report that the exit Mach number affects the losses through a modification of the pressure gradient imposed on the boundary layer. Boyle et al.[23] provide aerodynamic data for a linear turbine vane cascade, including surface pressure distributions and aerodynamic losses for different Reynolds numbers, Mach numbers, and levels of inlet turbulence. These investigations indicate that loss levels are fairly constant with the change of Mach number and are not sensitive to freestream turbulence level.

The present study focuses on the effects of surface roughness, freestream Mach number, and turbulence intensity levels on aerodynamic losses downstream of symmetric turbine airfoils in compressible, high-speed flow. The present study is different from the other investigations mentioned because the combined effects of surface roughness, mainstream Mach number, and turbulence intensity level are considered as they affect aerodynamic performance. The presence and development of shock waves for the transonic case are also discussed, along with shock wave changes that occur as the level of surface roughness changes. Three symmetric airfoils are employed, with different rough surfaces, which are characterized using equivalent sand grain roughness size. Magnitudes of equivalent sand grain roughness size for each surface are determined using three-dimensional optical profilometry data and procedures described by van Rij et al.[5] Exit freestream Mach numbers measured one chord length downstream of the airfoil are 0.6, 0.8, and 0.9. The magnitudes of longitudinal turbulence intensity used at the inlet of the test section are 0.9, 5.5, and 16.2%, where the latter values are produced using a mesh grid and cross bars, respectively.

Experimental Apparatus and Procedures

Transonic Wind Tunnel

The University of Utah Transonic Wind Tunnel (TWT) produces Mach numbers, pressure variations, Reynolds numbers, passage mass flow rates, and scaled physical dimensions that match values along airfoils in operating aeroengines and in gas turbines used for utility power generation. The TWT blowdown-type facility consists of two main parts: 1) compressor and storage tanks and 2) wind tunnel. The wind tunnel consists of five major subsections: 1) flow rate and pressure level management apparatus; 2) plenum tank; 3) inlet ducting and test section; 4) plenum, exit ducting, and ejector; and 5) control panel. A schematic diagram of this facility is given by Zhang et al.[24] More detailed descriptions are provided by Jackson et al.[25] and Furukawa and Ligrani.[26]

A Gardner Denver Company Model RL-1155-CB compressor is used to pressurize the array of eight tanks whose total capacity volume is 11.9 m^3. A VanAir VAS93039 Model D16-5 Deliquescent desiccant dryer, a Pall Corporation 5EHG-4882-207 oil filter, and two Permanent Filter Corporation 13846 particulate filters are located just downstream of the compressor to remove particulates and moisture from the air. A Fisher pressure regulator with a 6×4 EWT design sliding gate valve, a Fisher type 667 diaphragm actuator, a 3582 series valve positioner, and a Powers 535 process controller are used to regulate the pressure in the facility as the storage tanks discharge. A plenum tank, a 30.48-cm-inner-diameter pipe, a circular-to-square transition duct, a nozzle, and the test section then follow the pressure regulator.

Relative humidity at the test section inlet is typically 20–30%. The test section is connected to a large 92.71 by 91.44 by 91.44 cm^3 plenum with a square plastic flange at its outlet. The plenum diffuses high-speed air from the test section exit into a reservoir of low-velocity air. This plenum is then connected to two ducts, which are subsequently connected to the atmosphere. The facility also includes a Leister Model 8D8A-type 10,000 S electrical heater for heating of the mainstream air.

Pressure and Temperature Measurements

As tests are conducted, Validyne Model DP15-46 pressure transducers (with diaphragms rated at either 345 or 1380 kPa) and calibrated copper–constantan thermocouples are used to sense pressures and temperatures at different locations throughout the facility. Signals from the transducers are processed by Celesco Model CD10D carrier demodulators. All pressure transducer measurement circuits are calibrated using a Wallace and Tiernan FA145 bourdon tube pressure gauge as a standard. A United Sensor PLC-8-KL pitot-static probe with an attached copper–constantan thermocouple and a four-hole conical-tipped pressure probe with an attached copper–constantan thermocouple are used to sense total pressure, static pressure, and recovery temperature at the inlet and exit of the test section, respectively, during each blowdown. The four-hole probe has a tip that is 1.27 mm in diameter and a stem 3.18 mm in diameter. Each port has a diameter of 0.25 mm. The overall response time of the pressure measuring system is about 0.2 s. Mach numbers, sonic velocities, total temperatures, and static temperatures are determined from these data. The conical probe is aligned using two yaw ports placed on either side of the probe. As a blowdown is underway, the probe is located one chord length downstream of the airfoil. It is traversed using a two-axis traversing sled with two Superior Electric M092-FF-206 synchronous stepper motors, connected to a Superior Electric Model SS2000I programmable motion controller and a Superior Electric Model SS2000D6 driver. Commands for the operation of the motion controller are provided by LABVIEW 6.1 software and pass though a serial port after they originate in a Dell Precision 530 personal computer workstation.

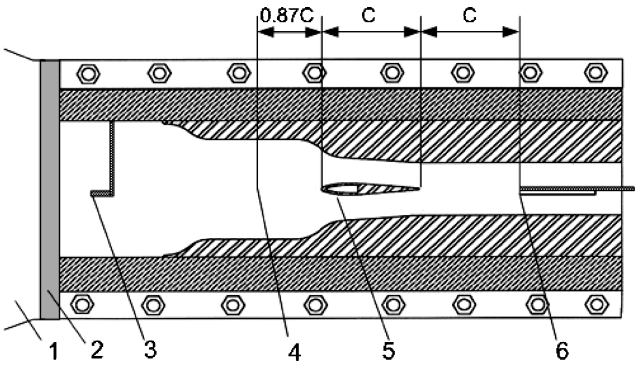

Fig. 1 Schematic diagram of the test section (from Zhang et al.[24]): 1) nozzle, 2) grid/bar turbulence generator, 3) inlet pressure probe and thermocouple, 4) measurement location for inlet turbulence intensity and flow uniformity, 5) test airfoil, and 6) exit pressure probe and thermocouple.

Voltages from the carrier demodulators and thermocouples are read sequentially using Hewlett–Packard HP44222T and HP44222A relay multiplexer card assemblies, installed in a Hewlett–Packard HP3497A low-speed data acquisition/control unit. This system provides thermocouple compensation electronically such that voltages for type-T thermocouples are given relative to 0°C. The voltage outputs from this unit are acquired by the Dell Precision 530 personal computer workstation through its universal serial bus (USB) port, using LABVIEW 6.1 software and a 188417D-01 GPIB-USB-B adaptor made by National Instruments.

Test Section

A schematic diagram of the nonturning airfoil cascade test section is shown in Fig. 1. The inlet of the test section is 12.70 by 12.70 cm. The ratio of inlet to exit area is about 2.5. The test section is made up of two acrylic side walls and top and bottom walls made of steel and acrylic. The two side walls are flat, whereas the top and bottom walls are contoured to form a converging–diverging shape, which produces the desired Mach number distribution along the symmetric test airfoil. Because significant flow turning is not included, the camber curvature, present in many cascades with multiple airfoils, is not present. Additional details are provided by Zhang et al.[24]

The present test section is useful for the following reasons: 1) The test section produces Mach numbers, pressure variations, Reynolds numbers, passage mass flow rates, and physical dimensions that match values along airfoils in operating engines. 2) The airfoil provides the same suction surface boundary-layer development (in the same pressure gradient without flow turning) as exists in operating engines. 3) Only one airfoil is needed to obtain representative flow characteristics. Thus, the present experiment is designed to isolate the effects of Mach numbers, surface roughness, and turbulence intensity on wake aerodynamic losses, while matching Reynolds numbers, Mach numbers, pressure gradients, passage flow rates, boundary-layer development, and physical dimensions of airfoils in operating engines.

Augmenting Mainstream Flow Turbulence Levels

Three different arrangements are used at the inlet of the test section to produce three different levels of mainstream turbulence intensity: 1) no grid or bars, 2) fine mesh grid, and 3) cross bars. The fine mesh grid consists of an array of four square rods arranged horizontally and four square rods arranged vertically. Each rod is spaced 25.4 mm from adjacent rods and is 5 mm on each side. The open area amounts to 48% of the inlet area. The cross-bars device consists of two parallel bars, where each is 25.4 mm in width, with 25.4 mm spacing from the adjacent bar, and 25.4 mm spacing from the top and bottom walls of the inlet duct. The open area amounts to 60% of the inlet area.

Longitudinal Turbulence Intensity Measurements

A single, horizontal-type platinum-plated tungsten hot-wire sensor, with a diameter of 12.7 μm and a length of 2.54 mm, is employed to measure the time-varying longitudinal component of velocity at the inlet of the test section. The time-averaged longitudinal velocity, longitudinal turbulence intensity, and turbulence length scale are then determined from these measurements. The mount for the hot-wire probe is attached to an airfoil, which is employed only for this purpose. With this arrangement, the hot-wire sensor is located 6.6 cm (or 87% of one chord length) upstream of the airfoil leading edge. The contraction ratio of the channel from this location to the leading edge is about 1.3. This position is 16.9 cm downstream of the turbulence generator. Note that inlet pressures are also measured at this location when the turbulence generating devices are installed. The vertical position of the probe, relative to the airfoil centerline, is adjustable so that the spatial uniformity of the flow can be checked at this streamwise location.

The hot-wire probe is driven by a Disa 55M10 constant-temperature hot-wire anemometer bridge with an overheat ratio of 1.6. The analog signal from this bridge is then processed using a Dantec 56N20 signal conditioner with a low-pass, antialiasing filter set to 100 kHz. The time-varying output voltage signal is then sampled at a 200-kHz rate using a DATEL PCI441D I/O board installed in the Dell Precision 530 personal computer workstation. During each measurement, 1,000,000 voltage values are sampled over a 5-s period. Data are acquired using LABVIEW 6.1 software and then processed further using MATLAB® 6.1 software, including determination of the turbulence length scale. This is accomplished by integrating the autocorrelation functions, which are deduced from the time-varying longitudinal velocity signals. The entire measurement system, including the hot-wire sensor, is calibrated in the freestream of the TWT. A Kiel-type pressure probe, wall static taps, and a copper–constantan thermocouple are used to measure and determine the total pressure, static pressure, recovery temperature, and velocity at the inlet of the test section as the calibration is conducted.

Test Airfoil and Surface Roughness

A schematic diagram of the cross section of one symmetric airfoil tested is shown in Ref. 24. The airfoil chord length c is 7.62 cm. The leading edge diameter is 0.3 cm, and the span width of the passage is 12.7 cm. The effective pitch p is 5.08 cm. The trailing edge of the symmetric airfoil is a 1.14-mm-radius round semicircle. Additional details are provided by Zhang et al.[24] Geometric dimensions of the contoured test walls and airfoil are given by Jackson.[27]

Three different airfoils, all with the same exterior dimensions but with different surface roughness characteristics, are used. One airfoil has a smooth surface, and the two other airfoils have rough surfaces. The roughness simulates the actual roughness that develops on operating turbine airfoils, over long operating times, due to particulate deposition and to spallation of thermal barrier coatings (TBCs). The roughness is applied by bonding nickel particles, manufactured by Praxair Surface Technologies, Inc., to the airfoil surfaces. The airfoil with the smaller-sized roughness elements has Praxair T1166F particles, which range in size from 20 to 53 μm. The airfoil with the larger-sized roughness elements has Praxair NI-914 particles, which range in size from 88 to 149 μm. The bonding is implemented using a layer of Cotronics Corporation Duralco 132 aluminum-filled, high thermoconductivity epoxy. The epoxy (and the roughness particles) are applied to an indented region located across the central span of the airfoil, which means that the mean level of the roughness is at the same level as the surrounding smooth surface. This approach is used to give the same exterior dimensions to the surfaces of all three airfoils, regardless of whether their surfaces are smooth or rough.

Experimental Uncertainties

Uncertainty estimates are based on 95% confidence levels and determined using procedures described by Kline and McClintock[28] and by Moffat.[29] Mach number uncertainty is ± 0.002. Uncertainty of temperatures is 0.15°C. Pressure uncertainty is 0.25 kPa. Uncertainties of C_p, $M_e/M_{e,\infty}$, and normalized kinetic energy KE are ± 0.0013 (0.07), ± 0.0023 (0.96), and ± 0.03 (0.90), respectively, where typical nominal values of these quantities are given in parenthesis. Integrated aerodynamic losses (IAL) uncertainty is ± 0.04 N/cm

(0.800 N/cm). Magnitudes of IAL, determined from replicate runs, are always within IAL uncertainty ranges.

TWT Qualifying Characteristics and Mainstream Airflow Conditions

Mach number distributions, measured along the airfoil, are shown in Fig. 2 and are similar to transonic values present on turbine airfoil suction surfaces for $P_{0i} = 195$ kPa. The Mach number distributions over the downstream half of the airfoil for P_{0i} of 140 and 114 kPa are approximately constant with x/c. These isentropic values are based on measurements of total pressure at the test section inlet and surface static pressures measured along the midspan line of a smooth airfoil, which is employed especially for this task. The eight measured values shown in Fig. 2 are based on measurements made along the top of surface of the smooth airfoil at freestream $Tu = 0.9\%$. These values are in excellent agreement with Mach numbers measured at three different locations on the bottom surface of the airfoil.

During each test, the inlet total pressure at the inlet of the test section, P_{0i}, is kept constant at one of the different values, at either 114, 140, or 195 kPa. Corresponding exit freestream Mach numbers, measured one chord length downstream of the airfoil trailing edge, are 0.6, 0.8, and 0.9, respectively, and chord Reynolds numbers (based on exit flow conditions) are 1.02×10^6, 1.38×10^6, and 1.96×10^6, respectively. With the highest inlet total pressure and the smooth airfoil, the flow in the passage is transonic and the trailing edge Mach number is 1.1. With this arrangement, a finite region of supersonic flow exists near the downstream portion of the airfoil, and a pair of oblique shock waves are present at the airfoil trailing edge.

With no turbulence grid employed at the test section inlet, the magnitude of the longitudinal turbulence intensity is 0.9%. Here, turbulence intensity is defined as the ratio of the root mean square of the fluctuation velocity component over the mean component. With the fine mesh turbulence-generating grid, the intensity and length scale are 5.5% and 15.24 mm, respectively. With the cross-bar turbulence-generating grid, the intensity and length scale are 16.2% and 19.70 mm, respectively. As mentioned, these values are measured for all three P_{0i} values at a location that is 87% of one chord length upstream of the airfoil leading edge and at an inlet Mach number of 0.24 and an inlet Reynolds number based on chord length of 0.54×10^6. For each of the three different values of inlet total pressure, magnitudes of turbulence intensity and turbulence length scale are about the same because they are mostly a result of the specific turbulence generator employed. During each blowdown test, these conditions can be maintained in the test section for up to 45-s time intervals. Such characteristics are not only due to the TWT design, but also to the excellent performance characteristics of the TWT mainstream air pressure regulator and its controller. Note that multiple blowdowns are required to complete each wake profile.

With no turbulence grid employed, the total pressure and static pressure show excellent spatial uniformity at the inlet of the test section because values vary by less than 1.38 kPa (or 0.7% of mean values) as measurements are made at nine different probe locations for $P_{0i} = 195$ kPa. Mach numbers determined from these data then vary by less than 0.002. Similar variations are also measured at a location that is 87% of one chord length upstream of the airfoil leading edge.

Recall that the location of the probe with respect to the airfoil can be varied. The variation of longitudinal turbulent intensity level measured at three pitchwise different locations is about 0.3% for the fine mesh grid. Slightly larger variations of about 1.4% are present when the cross bars are used to augment turbulence intensity levels. These measurements are positioned at a streamwise location that is 87% of one chord length upstream of the airfoil leading edge. The vertical positions of the hot-wire probe employed, relative to the airfoil centerline, are 0, 12.7, and 25.4 mm (in the pitchwise dimension) above the test section centerline.

Such spatial nonuniformities, if present, are compensated by the procedures employed to measure profiles of normalized local total pressure losses C_p, normalized local Mach numbers $M_e/M_{e,\infty}$, and normalized local KE. With either mesh grid or bars employed, this is accomplished by measuring these profiles both with and without an airfoil located in the test section. Differences in measured quantities for these two conditions then provide information on the effects of the airfoil and its surface condition, irrespective of any nonuniformities produced by the turbulence generating device that is used.

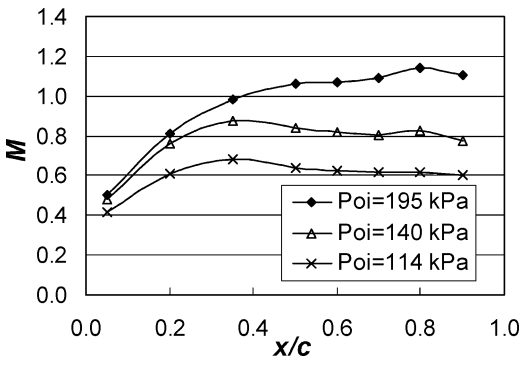

Fig. 2 Airfoil Mach number distributions for smooth airfoil with low freestream turbulence level $Tu = 0.9\%$.

Experimental Results and Discussion

Roughness Characterization

The magnitudes of equivalent sandgrain roughness are determined for all three surfaces tested using procedures that are described by van Rij et al.[5]

The first step in this approach is a detailed determination of surface contour coordinates using a Wyko high-resolution optical Surface Profilometer. Figure 3a shows an enlarged image of a portion of the test surface with small-sized roughness elements, obtained from optical profilometry data. The image of a rough surface from the pressure side of a turbine blade with particulate deposition from a utility power engine is shown in Fig. 3b. The similarity of irregularity, nonuniformity, and three-dimensional nature of the roughness elements, including their irregular arrangement, are evident from Figs 3. Equivalent sand grain roughness size of this real turbine blade surface is about 62.3 μm, which is close to the size of test surface of small-sized roughness elements (52.59 μm). Table 1 also show that magnitudes of other surface roughness statistics from the utility power engine turbine blade are also similar to test surfaces employed with small-sized and large-sized roughness elements.

The next step in the procedure to determine equivalent sand grain roughness magnitudes is numerical determination of a modified version of the Sigal and Danberg roughness parameter Λ_s (see Refs. 3–5). The procedures to accomplish this are described by van Rij et al.[5] and involve determination of the rough surface flat reference area S, the total roughness frontal area S_f, and the total roughness windward wetted surface area S_s. This parameter is then given by

$$\Lambda_s = (S/S_f)(S_f/S_s)^{-1.6}$$

With Λ_s known, the ratio of equivalent sand grain roughness size to mean roughness height, k_s/k, is determined using a correlation for three-dimensional, irregular roughness with irregular geometry and

Table 1 Characteristics of rough surfaces investigated

Surface	Λ_s	k_s/k	k, μm	k_s, μm	k_s/c
Large-sized roughness	15.447	1.959	64.03	125.19	0.00164
Small-sized roughness	20.101	1.889	27.92	52.59	0.00069
Smooth	3020.7	.0026	3.50	.0094	0
Turbine blade from a utility power engine	43.455	1.641	40.815	62.30	0.00082

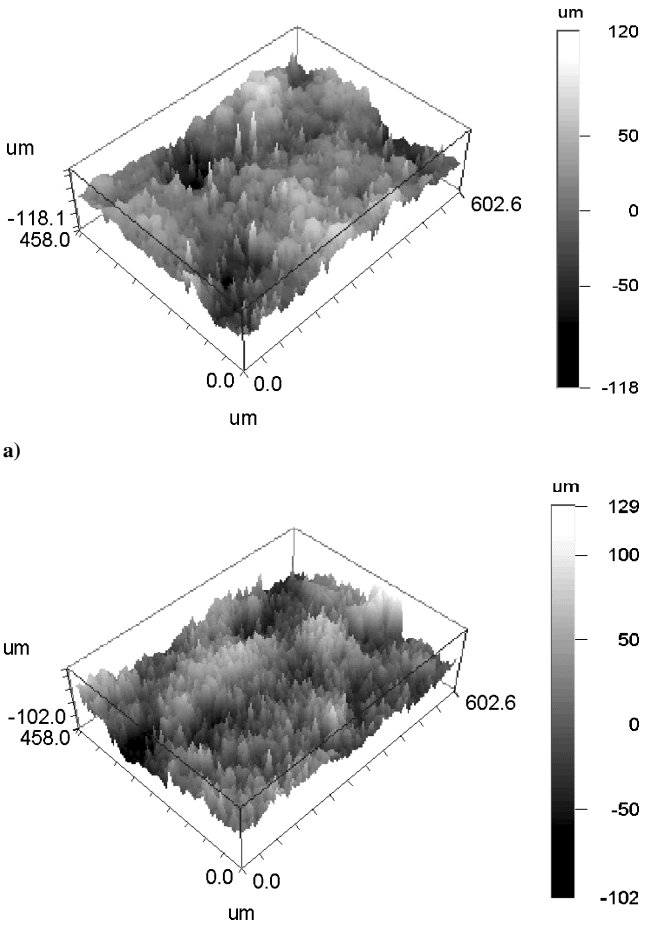

Fig. 3 Three-dimensional Wyko profilometry traces of portions of rough surfaces: a) simulated rough surface with small-sized roughness elements, and b) rough surface from pressure side of turbine blade with particulate deposition from a utility power engine (from Zhang et al.[24]).

arrangement, which is given by van Rij et al.,[5]

$$\frac{k_s}{k} = \begin{cases} 1.584 \times 10^{-5}\Lambda_s^{5.683} & \Lambda_s \le 7.842 \\ 1.802\Lambda_s^{0.0304} & 7.842 \le \Lambda_s \le 28.12 \\ 255.5\Lambda_s^{-1.454} & 28.12 \le \Lambda_s \end{cases} \quad (1)$$

The mean roughness height k is then also estimated by taking the distance between the maximum point of the ensemble average of all of the roughness peaks in any roughness sample and a base height. Determination of this base location is based on analytic procedures, which are also given by van Rij et al.[5]

With this approach, magnitudes of equivalent sand grain roughness size for the three-dimensional, irregular roughness of the present study are determined. Values are given in Table 1, which are based on an average of eight profilometry scans. The variation of k_s/k is 3% among eight traces for the surface with the large-sized roughness and 2.6% among six traces for the surface with the small-sized roughness. Note that all parameters listed in Table 1 are approximately matched by the small-sized roughness used in the present experiments. Magnitudes of Λ_s and k_s/k from the present study are also shown in Fig. 4, along with Eq. (1) and values from the Schlichting,[2] Sigal and Danberg,[3] and van Rij et al.[5] investigations. Also included in Fig. 4 is the correlation for two-dimensional roughness from Sigal and Danberg.[3] Note also that the trend of their data for three-dimensional roughness is very close to the line from van Rij et al.[5] also for $\Lambda_s \ge 28.12$ shown in Fig. 4.

Local Aerodynamic Performance

Figures 5–8 present local aerodynamic performance data in the wake for various experimental conditions: three surface roughness

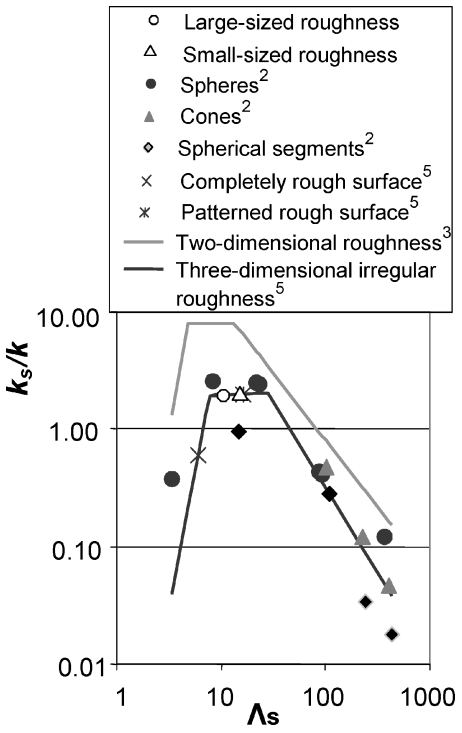

Fig. 4 Dependence of ratio of equivalent sand grain roughness size to mean roughness height on the Sigal and Danberg[3,4] roughness parameter for the present study, the Schlichting[2] investiation, and the van Rij et al.[5] investigations (from Zhang et al.[24]).

sizes, three levels of exit freestream Mach number, and three freestream turbulence intensity levels. Combined effects of these parameters are also discussed.

Figures 5a–5c show the effects of surface roughness on normalized local total pressure losses C_p, normalized local Mach numbers $M_e/M_{e,\infty}$, and normalized local KE profiles for an inlet turbulence intensity level of 0.9%. Data are given for k_s/c values of 0, 0.00069, and 0.00164, which correspond to the smooth, small-sized roughness, and large-sized roughness, respectively. The inlet total pressure is kept constant at 195 kPa when different airfoils are employed. The results in Figs. 5 are given for an exit freestream Mach number 0.9 and for a low value of inlet turbulence intensity because variations due to roughness are often generally more apparent than for higher inlet turbulence intensity levels. Figure 5 shows that total pressure losses, Mach number deficits, and deficits of KE all increase at each y/c location as k_s/c increases. This is apparent at peak value locations and is accompanied by increases in the width of the profiles as roughness size becomes larger. This is largely due to increased thickening of the boundary layers along the airfoil surfaces as k_s/c increases, which is accompanied by higher magnitudes of Reynolds stress tensor components, higher magnitudes of local turbulent transport, and higher surface skin-friction coefficients. The broader wakes with increased roughness size in Fig. 5 are then the result of 1) augmentations of mixing and turbulent transport in the boundary layers, which develop along the roughened airfoils; 2) thicker boundary layers at the airfoil trailing edges of the roughened airfoils; and 3) increased turbulent diffusion in the transverse direction within the wake as it advects downstream. For the present airfoil shape and configuration, numerical predictions by Zhang et al.[30] show that flow separation regions (as well as associated form drag contributions) are about the same for all three airfoils, regardless of their k_s/c value (of either 0, 0.00069, or 0.00164). Numerical results also show that boundary layers are almost entirely turbulent along the entire length of all three tested airfoils. From these numerical predictions, values of k_s^+ just before the airfoil trailing edge for $M_{e,\infty} = 0.6$, normalized by friction velocity and kinetic viscosity, are approximately 24.8 and 60.9 for the small-sized roughness and large-sized roughness, respectively.

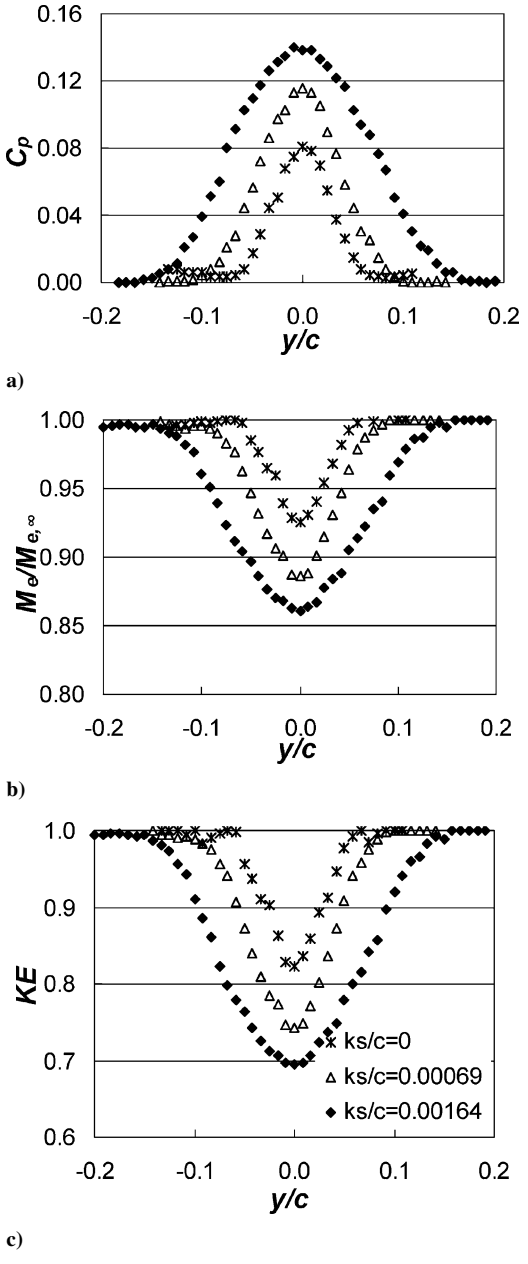

Fig. 5 Profiles measured with $M_{e,\infty} = 0.9$ and $Tu = 0.9\%$: a) normalized local total pressure losses, b) normalized local Mach numbers, and c) normalized local KE.

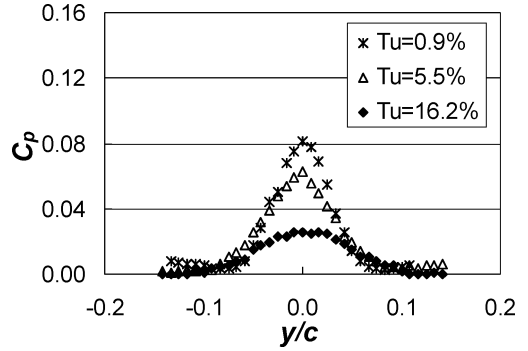

Fig. 6 Normalized local total pressure losses profiles measured using smooth airfoil ($k_s/c = 0$) with different turbulence intensity levels for $M_{e,\infty} = 0.9$.

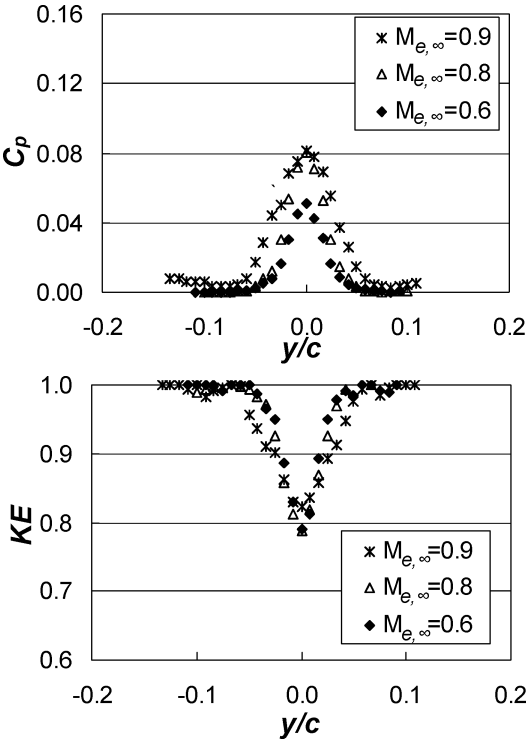

Fig. 7 Normalized local total pressure losses profiles and normalized KE profiles measured using the smooth airfoil ($k_s/c = 0$) with different Mach numbers for $Tu = 0.9\%$.

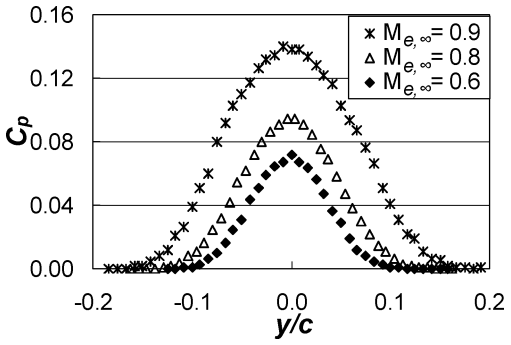

Fig. 8 Normalized local total pressure losses profiles measured using the airfoil with large-sized roughness ($k_s/c = 0.00164$) with different Mach numbers for $Tu = 0.9\%$.

Other changes due to surface roughness are apparent in the C_p values in Fig. 5a for $M_{e,\infty} = 0.9$, which are measured in the freestream flow outside of the wake. With the smooth airfoil, the C_p values in the freestream are approximately 0.0030–0.007, which correspond to $(P_{0i} - P_{0e,\infty})$ values of 0.4–1.4 kPa. The resulting difference in stagnation pressure between the inlet and exit of the test section is due to a pair of oblique shock waves present at the trailing edge of the airfoil. With a similar experimental condition, Jackson et al.[25] report similar $C_{p,\infty}$ values, which result from strong oblique shock waves at the airfoil trailing edge with angles relative to the axial direction of about 73 deg. Their schlieren results show that no shock waves are present in front of the exit pressure probe. With roughness on the airfoil surface, the boundary layers that develop along the airfoil are much thicker. As a result, blockage of the flow in the airfoil passage is increased, with less flow expansion as it advects through the test section passage. Consequently, the Mach number along the roughened airfoil is different, the flow in the passage is entirely subsonic, and the maximum Mach number is about 0.9. No trailing-edge shock waves are then present at the trailing edge of the roughened airfoil, freestream $C_{p,\infty}$ values are zero, and P_{0i} is approximately equal to $P_{0e,\infty}$.

Figure 6 shows the effects of different inlet freestream turbulence levels on normalized local total pressure losses C_p profiles for the smooth airfoil with $M_{e,\infty} = 0.9$ and $k_s/c = 0$. Results are presented for Tu magnitudes of 0.9, 5.5, and 16.2%. As the inlet turbulence intensity increases, distributions of C_p show that the wake downstream of the airfoil becomes slightly wider. At the center of the wake at $y/c = 0$, C_p values drop dramatically as inlet turbulence intensity increases. In their low-speed cascade experiments, Ames and Plesniak[18] also observe wake broadening with increasing mainstream turbulence intensity and associate these with smaller peak velocity deficits. Increased diffusion from the wake to surrounding freestream flow plays an important role in producing such trends. Note that increased losses are present in the freestream as freestream turbulence level increases in the experiments of Ames and Plesniak.[18] These freestream losses appear to be more important than the reduced losses observed within the wake and, as such, have important effects on overall loss magnitudes. As a result, elevated freestream turbulence intensity levels substantially increase their mass-averaged loss coefficients. However, if wake losses only are considered, the aerodynamic losses reported by Ames and Plesniak decrease as freestream turbulence level is elevated, just as in the present investigation. In the present study, a symmetric airfoil is used with a zero angle of inclination. The total pressure measured at inlet of the test section is almost the same as the total pressure in the freestream at the outlet, which means the freestream losses are negligible. Boyle et al.[23] also find negligible freestream losses in their high-speed cascade experiments, but they present significantly different trends from Ames and Plesniak,[18] as well as the present study, because peak total pressure loss magnitudes increase as the level of mainstream turbulence increases. In addition, the exit measurement location used in the present study is much farther downstream of the airfoil compared to the measurement locations employed by Ames and Plesniak[18] and Boyle et al.[23] (Note that they[18,23] use curved ducts, whereas the present study uses a straight duct.) The results of Ames and Plesniak[18] are given for a location that is 20% of the axial chord length, or 35% of the true chord length, downstream of the airfoil. For the Boyle et al. study,[23] this location is 35% of the axial chord length, whereas 100% is employed in the present investigation. In near-wake region (just downstream of an airfoil), increased freestream turbulence levels increase airfoil surface skin-friction coefficients giving thickened trailing-edge boundary layers and stronger wake strengths. Wake strengths and deficits of total pressure are more likely to decrease as freestream turbulence level increases in the far-wake region because of the influences of turbulent diffusion of momentum from the wake to the surrounding fresstream flow.

Figure 7 shows the effect of Mach number on normalized local total pressure losses C_p profiles for the smooth airfoil with $k_s/c = 0$ and $Tu = 0.9\%$. Distributions of C_p show that the wake downstream of the airfoil becomes wider with larger total pressure deficits as the freestream Mach number increases. Wider C_p profiles are a result of higher advection speeds, as well as increased diffusion within the wake. Note also that freestream C_p values are nonzero for $M_{e,\infty} = 0.9$ because of trailing-edge shock waves. The change of the Mach number distribution along the airfoil also affects the pressure gradient imposed on the boundary layer. Compressibility, which becomes more important at higher freestream Mach numbers, produces additional alterations to the character and development of boundary layers. Also shown in Fig. 7 is the normalized KE profile, which appear to be less sensitive (than C_p profiles) to changes of the airfoil Mach number distribution.

Figure 8 presents the same type of data as are shown in Fig. 7, also for Tu magnitudes of 0.9%, except that these data are obtained with large-sized roughness ($k_s/c = 0.00164$) along the airfoil surface. These results, thus, illustrate the combined effects of Mach number and airfoil surface roughness on aerodynamic losses. A comparison of profiles in Figs. 7 and 8 show that C_p distributions are less sensitive to Mach number variations when the airfoil is smooth. The data in Fig. 8 show much larger C_p variations as the exit freestream Mach number is varied. This means that the Mach number has a greater effect on the thicker boundary layers that develop over rough airfoil surfaces, where turbulent mixing and turbulent transport are also increased relative to smooth airfoil surface boundary layers.

Integrated Aerodynamic Losses

Dimensional magnitudes of IAL are determined by integrating profiles of $(P_{0e,\infty} - P_{0e})$ with respect to y in the transverse flow direction across the wake. Integrated aerodynamic losses (IAL) magnitudes are determined from profiles that are measured one chord length downstream of the airfoil. Consequently, IAL magnitudes represent mixing losses that have accumulated through the wake and airfoil boundary layers that are located upstream.

Such IAL magnitudes are presented in Fig. 9 as dependent on the inlet turbulence intensity level for the airfoils with the smooth surfaces ($k_s/c = 0$), small-sized roughness ($k_s/c = 0.00069$), and large-sized roughness ($k_s/c = 0.00164$). When the turbulent intensity levels increase from 0.9 to 5.5%, IAL magnitudes decrease for all three cases with airfoils with different surface roughness. Different trends for various k_s/c values are found as the turbulent intensity levels increase from 5.5% to a much higher value, 16.2%. For the smooth airfoil, IAL continuously decreases as the magnitude of the inlet turbulence intensity increases. For the airfoil with the small-sized roughness ($k_s/c = 0.00069$), the magnitudes of IAL become less sensitive to Tu and are nearly kept constant while Tu increases from 5.5 to 16.2%. For the airfoil with large-sized roughness ($k_s/c = 0.00164$), IAL magnitudes increase slightly as the inlet turbulence intensity level gets larger. These trends indicate that the effects of turbulence intensity level on IAL magnitudes are also dependent on the level of surface roughness, k_s/c. Some of the variations shown by the data in Fig. 9 are connected, at least in part, to different airfoil Mach number distributions with and without roughness and to the presence of trailing-edge shock waves, which are present only at the downstream of the smooth airfoil.

IAL data are normalized using the airfoil passage effective pitch p and test section inlet stagnation pressure P_{0i} in Fig. 10. These data are given because they depend on k_s/c for different Tu values. The overall trends of the data in Fig. 10 illustrate the dominating influences of airfoil surface roughness on aerodynamic losses and the weaker dependence of these losses on inlet freestream turbulence intensity level. The data in Fig. 10 also show larger IAL variations with Tu at the largest k_s/c value, which provides additional evidence that thicker rough-surface boundary layers are more sensitive to changes of freestream turbulence level than thinner boundary layers that develop over smooth surfaces.

Figure 11 shows how normalized IAL data vary with exit freestream Mach number for different values of k_s/c. Here, IAL values increase as the exit freestream Mach number increases for each value of k_s/c. This is consistent with results from Christopher et al.[21] and Xu and Denton,[31] whose experimental and analytical results show that total pressure losses increase approximately with the

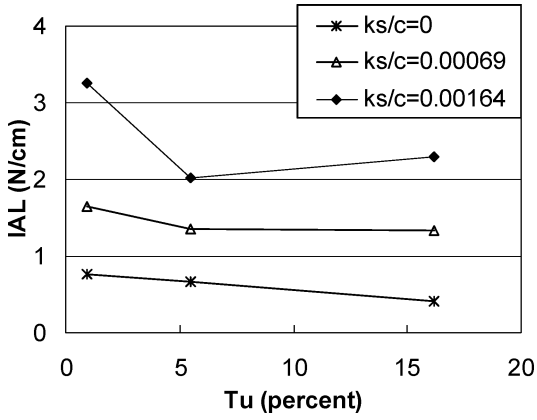

Fig. 9 For $M_{e,\infty} = 0.9$, comparison of dimensional IAL as dependent on the inlet turbulence intensity level for the smooth airfoil ($k_s/c = 0$), the airfoil with small roughness ($k_s/c = 0.00069$), and the airfoil with large roughness ($k_s/c = 0.00164$).

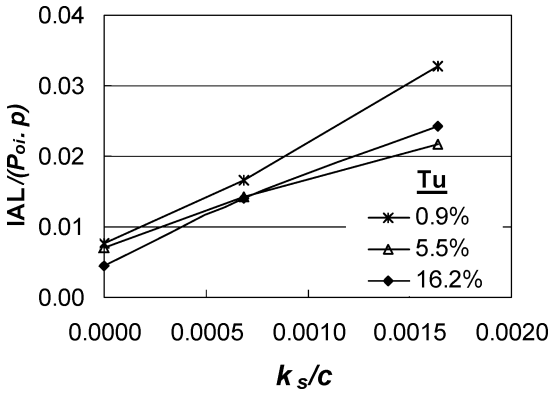

Fig. 10 Comparison of normalized IAL as dependent on normalized equivalent sand grain roughness size for different inlet turbulence intensity levels for $M_{e,\infty} = 0.9$.

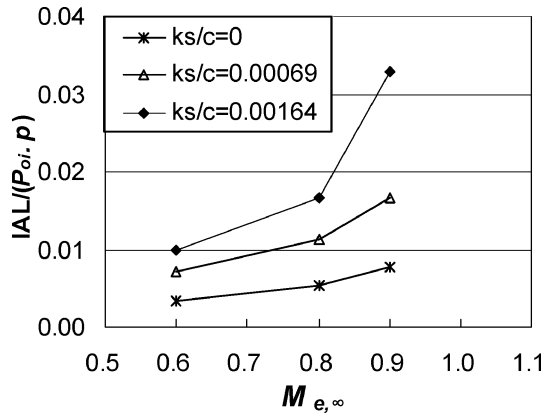

Fig. 11 For $Tu = 0.9\%$, comparison of dimensional IAL as dependent on the exit Reynolds number for the smooth airfoil ($k_s/c = 0$), the airfoil with small roughness ($k_s/c = 0.00069$), and the airfoil with large roughness ($k_s/c = 0.00164$).

square of the Mach number. Figure 11 also shows that the largest IAL magnitude increases with Mach number are present with the large-sized roughness ($k_s/c = 0.00164$). Overall, such data further illustrate different dependence of aerodynamic losses on exit freestream Mach number, which occur as the level of airfoil surface roughness changes.

Summary

The effects of surface roughness, freestream Mach number, and turbulence intensity on the aerodynamic performance of turbine airfoils are investigated. Wake profiles are measured with exit freestream Mach numbers of 0.6, 0.8, and 0.9 and three different inlet turbulence intensity levels of 0.9, 5.5, and 16.2%. Three symmetric airfoils, each with the same shape and exterior dimensions, are employed with ratios of equivalent sand grain roughness size to airfoil chord length k_s/c of 0, 0.00069 and 0.00164. For the latter two airfoils, the nonuniform, irregular, three-dimensional roughness is created to match the roughness that exists on operating turbine vanes and blades subject to extended operating times with significant particulate deposition on the surfaces.

Changing the airfoil surface roughness condition has a substantial effect on profiles of total pressure loss coefficients and on the normalized and dimensional magnitudes of IAL produced by the airfoils. The dependence of these losses on mainstream turbulence intensity and freestream Mach number is vastly different as level of airfoil surface roughness changes. For example, magnitudes of IAL change by much larger amount as either the freestream Mach number or turbulence intensity is altered, when the airfoil is roughened. This is partially a result of the thicker boundary layers, which develop over the roughened surfaces giving greater blockage and less expansion of the flow through the airfoil passage.

Total pressure losses in the freestream with transonic passage flow indicate that oblique shock waves are present at the trailing edge of the airfoil when the airfoil is smooth, which are not present when the airfoil surfaces become roughened. The thicker boundary layers that develop along the roughened airfoil cause greater passage flow blockage, with less flow expansion through the test section passage. Consequently, the Mach number along the roughened airfoil is different, the flow in the passage is entirely subsonic, and the maximum Mach number is about 0.9. No trailing-edge shock waves are then present at the trailing edge of the roughened airfoil, freestream $C_{p,\infty}$ values are zero, and P_{0i} is approximately equal to $P_{0e,\infty}$.

Acknowledgments

The research reported in this paper was sponsored by the National Science Foundation (NSF Grant CTS-0086011). Stefan Thynell and Richard Smith were the NSF Program Monitors. The authors also acknowledge Mike Blair of Pratt and Whitney Corporation, Hee-Koo Moon of Solar Turbines, Inc., Ed North and Ihor Diakunchak of Siemens–Westinghouse Corporation, and Richardo Trindade of Pratt and Whitney, Canada Corporation for guidance and suggestions on this research effort and for providing roughened turbine blade hardware from engines for analysis and comparison.

References

[1]Nikuradse, J., "Laws of Flow in Rough Pipes," NACA TM 1292, 1933.
[2]Schlichting, H., "Experimental Investigation of the Problem of Surface Roughness," NACA TM-832, 1936.
[3]Sigal, A., and Danberg, J. E., "New Correlation of Roughness Density Effect on Turbulent Boundary layer," *AIAA Journal*, Vol. 28, No. 3, 1990, pp. 554–556.
[4]Sigal, A., and Danberg, J. E., "Analysis of Turbulent Boundary Layer Over Roughness Surface With Application to Projectile Aerodynamics," Army Ballistic Research Lab, Tech. Rept. BRL-TR-2977, Aberdeen Proving Grounds, MD, 1988.
[5]van Rij, J. A., Belnap, B. J., and Ligrani, P. M., "Analysis and Experiments on Three-Dimensional, Irregular Surface Roughness," *Journal of Fluids Engineering*, Vol. 124, Sept. 2002, pp. 1–7.
[6]Bammert, K., and Sandstede, H., "Influence of Manufacturing Tolerances and Surface Roughness of Blades on the Performance of Turbines," American Society of Mechanical Engineers, ASME Paper 75-GT-35, 1975.
[7]Bammert, K., and Sandstede, H., " Measurements of the Boundary Layer Development along a Turbine Blade with Rough Surfaces," *Journal of Engineering for Power*, Vol. 102, Oct. 1980, pp. 978–983.
[8]Kind, R. J., Serjak, P. J., and Abbott, M. W. P., "Measurements and Prediction of the Effects of Surface Roughness on Profile Losses and Deviation in a Turbine Cascade," American Society of Mechanical Engineers, ASME Paper 96-GT-203, 1996.
[9]Bogard, D. G., Schmidt, D. L., and Tabbita, M., "Characterization and Laboratory Simulation of Turbine Airfoil Surface Roughness and Associated Heat Transfer," *Journal of Turbomachinery*, Vol. 120, July 1998, pp. 337–342.
[10]Abuaf, N., Bunker, R. S., and Lee, C. P., "Effects of Surface Roughness on Heat Transfer and Aerodynamics Performance of Turbine Airfoils," *Journal of Turbomachinery*, Vol. 120, 1998, pp. 522–529.
[11]Leipold, R., Boese, M., and Fottner, L., "The Influence of Technical Surface Roughness Caused by Precision Forging on the Flow Around a Highly Loaded Compressor Cascade," *Journal of Turbomachinery*, Vol. 122, July 2000, pp. 416–425.
[12]Guo, S. M., Oldfield, M. L. G., and Rawlinson, A. J., "Influence of Discrete Pin Shaped Surface Roughness (P-Pins) on Heat Transfer and Aerodynamics of Film Cooled Aerofoil," American Society of Mechanical Engineers, ASME Paper GT-2002-30179, 2002.
[13]Geogory-Smith, D. G., and Cleak, J. G. E., "Secondary Flow Measurements in a Turbine Cascade with High Inlet Turbulence," *Journal of Turbomachinery*, Vol. 114, Jan. 1992, pp. 173–183.
[14]Hoffs, A., Drost, U., and Bolcs, A., "Heat Transfer Measurements on a Turbine Airfoil at Various Reynolds Numbers and Turbulence Intensities Including Effects of Surface Roughness," American Society of Mechanical Engineers, ASME Paper 96-GT-169, 1996.
[15]Giel, P. W., Bunker, R. S., Van Fossen, G. J., and Boyle, R. J., "Heat Transfer Measurements and Predictions on a Power Generation Gas Turbine Blade," American Society of Mechanical Engineers, ASME Paper 2000-GT-209, 2000.
[16]Boyle, R. J., Luci, B. L., Verhoff, V. G., Camperchioli, W. P., and La, H., "Aerodynamics of a Transitioning Turbine Stator Over a Range of Reynolds Numbers," American Society of Mechanical Engineers, ASME Paper 98-GT-285, 1998.

[17]Nix, A. C., Smith, A. C., Diller, T. E., Ng, W. F., and Thole, K. A., "High Intensity, Large Length-scale Freestream Turbulence Generation in a Transonic Turbine Cascade," American Society of Mechanical Engineers, ASME Paper GT-2002-30523, 2002.

[18]Ames, F. E., and Plesniak, M. W., "The Influence of Large–Scale, High Intensity Turbulence on Vane Aerodynamics Losses, Wake Growth, and the Exit Turbulence Parameters," *Journal of Turbomachinery*, Vol. 119, April 1997, pp. 182–192.

[19]Jouini, D. B. M., Sjolander, S. A., and Moustapha, S. H., "Aerodynamic Performance of a Transonic Turbine Cascade at Off-Design Conditions," *Journal of Turbomachinery*, Vol. 123, July 2001, pp. 510–518.

[20]Radomsky, R. W., and Thole, K. A., "Detailed Boundary Layer Measurements on a Turbine Stator Vane at Elevated Freestream Turbulence Levels," *Journal of Turbomachinery*, Vol. 124, Jan. 2002, pp. 107–118.

[21]Christopher, R. J., Xavier, A. M., Friedrich, O. S., Charles, D. M., and Matthew, M., "High Pressure Turbine Vane Annular Cascade Heat Flux and Aerodynamic Measurements with Comparisons to Predictions," American Society of Mechanical Engineers, ASME Paper 98-GT-430, 1998.

[22]Coton, T., Arts, T., and Lefebvre, M., "Effects of Reynolds and Mach Numbers on the Profile Losses of a Conventional Low-Pressure Turbine Rotor Cascade with an Increasing Pitch–Chord Ratio," *Journal of Power and Energy*, Vol. 215, No. 6, 2001, pp. 763–772.

[23]Boyle, R. J., Lucci, B. L., and Senyitko, R. G., "Aerodynamics Performance and Turbulence Measurements in a Turbine Vane Cascade," American Society of Mechanical Engineers, ASME Paper GT-2002-30434, 2002.

[24]Zhang, Q., Lee, S. W., and Ligrani, P. M., "Effects of Surface Roughness and Turbulence Intensity on the Aerodynamic Losses Produced by the Suction Surface of a Simulated Turbine Airfoil," *Journal of Fluids Engineering*, Vol. 126, No. 2, March 2004.

[25]Jackson, D. J., Lee, K. L., Ligrani, P. M., and Johnson, P. D., "Transonic Aerodynamic Losses Due to Turbine Airfoil, Suction Surface Film Cooling," *Journal of Turbomachinery*, Vol. 122, April 2000, pp. 317–326.

[26]Furukawa, T., and Ligrani, P. M., "Transonic Film Cooling Effectiveness from Shaped Holes on a Simulated Turbine Airfoil," *Journal of Thermophysics and Heat Transfer*, Vol. 16, April–June 2002, pp. 228–237.

[27]Jackson, D. J., "Aerodynamic Mixing Losses and Discharge Coefficients Due to Film Cooling From a Symmetric Turbine Airfoil in Transonic Flow," M.S. Thesis, Dept. of Mechanical Engineering, Univ. of Utah, Salt Lake City, Aug. 1998.

[28]Kline, S. J., and McClintock, F. A., "Describing Uncertainties in Single Sample Experiments," *Mechanical Engineering*, Vol. 75, 1953, pp. 3–8.

[29]Moffat, R. J., "Describing the Uncertainties in Experimental Results," *Experimental Thermal and Fluid Science*, Vol. 1, 1988, pp. 3–17.

[30]Zhang, Q., Lee, S. W., and Ligrani, P. M., "Determination of Rough-Surface Skin Friction Coefficients from Wake Profile Measurements," *Experiments in Fluids*, Vol. 35, Oct. 2003, pp. 627–635.

[31]Xu, L., and Denton, J. D., "The Base Pressure and Loss of a Family of Four Turbine Blades," *ASME Journal of Turbomachinery*, Vol. 10, Jan. 1988, pp. 9–17.